Static capacitive pressure sensing using a single graphene drumg

Davidovikj, Dejan; Scheepers, Paul H.; Van Der Zant, Herre S.J.; Steeneken, Peter G.

DOI
10.1021/acsami.7b17487

Publication date
2017

Document Version
Accepted author manuscript

Published in
ACS Applied Materials and Interfaces

Static capacitive pressure sensing using a single graphene drum

Dejan Davidovikj[1],* Paul H. Scheepers[1], Herre S. J. van der Zant[1], and Peter G. Steeneken[1,2]

[1]*Kavli Institute of Nanoscience, Delft University of Technology, Lorentzweg 1, 2628 CJ Delft, The Netherlands*

[2]*Department of Precision and Microsystems Engineering, Delft University of Technology, Mekelweg 2, 2628 CD, Delft, The Netherlands*

E-mail: d.davidovikj@tudelft.nl

Abstract

To realize nanomechanical graphene-based pressure sensors, it is beneficial to have a method to electrically readout the static displacement of a suspended graphene membrane. Capacitive readout, typical in micro-electro-mechanical systems (MEMS), gets increasingly challenging as one starts shrinking the dimensions of these devices, since the expected responsivity of such devices is below 0.1 aF/Pa. To overcome the challenges of detecting small capacitance changes, we design an electrical readout device fabricated on top of an insulating quartz substrate, maximizing the contribution of the suspended membrane to the total capacitance of the device. The capacitance of the drum is further increased by reducing the gap size to 110 nm. Using external pressure load, we demonstrate successful detection of capacitance changes of a single graphene drum down to 50 aF, and pressure differences down to 25 mbar.

KEYWORDS

static capacitive readout, graphene drum, pressure sensor, minimizing parasitic capacitance, nanomechanics, two-dimensional materials

INTRODUCTION

Nanomechanical devices from suspended graphene and other two-dimensional materials have been receiving growing interest in the past few years for their potential as sensitive pressure[1–6] and gas[7–9] sensors. To realize integrated, small and low-power devices, it is necessary to have all-electrical on-chip transduction schemes, in contrast to the currently often employed laser interferometry techniques for the readout of their dynamic motion and static deflection.

Reports on electrical readout of graphene membrane nanomechanical devices have employed readout schemes based on electrical transconductance[6,10] and piezoresistivity.[1,2,4] Both of these rely on the change in the conductance of the membrane as a function of deflection, which is then used to sense the motion of the membrane. Although these methods can be very sensitive, the graphene conductance can also be affected by variations in gas composition, humidity, light intensity and temperature. Moreover, the conductance is not only related to the deflection of the graphene membrane, but depends also on material parameters like the electron mobility and piezoresistive coefficients. These approaches therefore require calibration and a high degree of stability of the graphene and insensitivity to variations in its surroundings.

In contrast, the capacitance between a graphene membrane and a bottom electrode is, to first order, a function only of the geometry of the system and, therefore, the deflection of the membrane. A measurement of the capacitance of the membrane can therefore be used to calculate its deflection, which makes capacitance detection an interesting alternative method

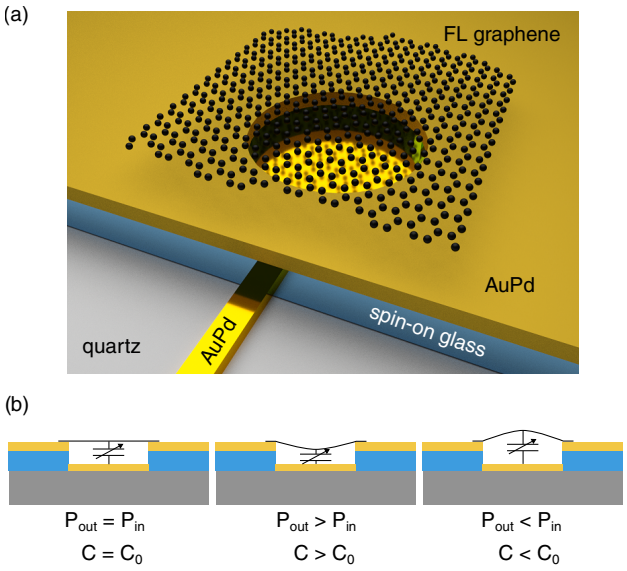

Figure 1: (a) A 3D schematic of the device: a capacitor is formed between a (few-layer) graphene drum suspended over a metallic cavity and a bottom metallic electrode that runs underneath an insulating (spin-on glass) oxide layer. The entire device is fabricated on top of an insulating quartz wafer. (b) Actuation principle: external pressure load is applied. Depending on the pressure difference between the cavity and the outside environment, the nanodrum will bulge upwards or downwards resulting in a decrease or increase of the measured capacitance.

for electrical readout of nanomechanical graphene sensors. Dynamic (on-resonance) capacitive readout has been demonstrated on suspended graphene bridges[11,12] and in suspended graphene nanodrums coupled to superconducting cavities at cryogenic temperatures.[13–15] The dynamic performance of such devices greatly deteriorates at room temperature and atmospheric pressure as the quality factor and therefore the motion amplitude at a given force are much smaller.[3,16,17] Capacitive readout of the *static* deflection of a graphene drum is hence a more viable solution for graphene-based devices operating in ambient conditions. This is, however, challenging to realize, mainly due to the on-chip parasitic capacitances that are usually much larger than the capacitance of the device and also because low-frequency measurements are more susceptible to noise. One way of tackling these issues is increasing the total capacitance of the device as proposed[18] and later realized[19] on a voltage tunable capacitor array comprised of thousands of unsealed graphene bridges in parallel.

Here we present capacitive detection of the static deflection of a *single* few-layer graphene

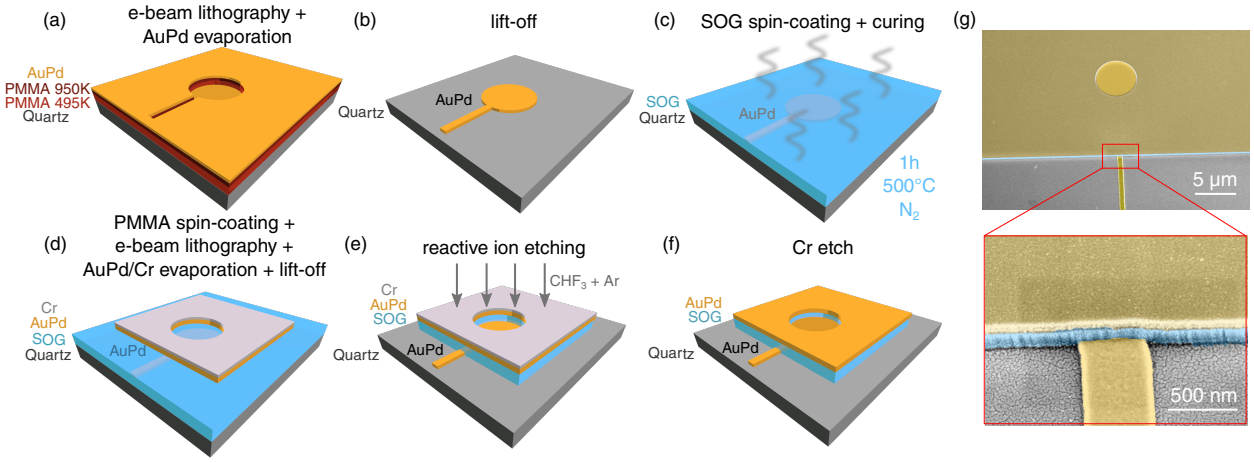

Figure 2: (a) - (f) Fabrication steps. (g) A false-colored SEM image of the device showing the top and bottom electrodes (yellow) and the separating SOG layer (blue). A zoomed-in image of the AuPd/SOG/AuPd interface is shown in the bottom panel.

drum enclosing a cavity, which allows us to benchmark its performance as a pressure sensor.

DEVICE CONCEPT AND FABRICATION

The total capacitance of a suspended graphene drum and the underlying electrode in typical sample geometries (circular drum 5-10 μm in diameter, suspended over a 300 nm-deep cavity), ranges from 0.5 to 2 femtoFarads. A displacement of such a drum of 1 nm would result in a capacitance change of only 2-6 attoFarads. Fabricating readout circuitry sensitive enough to detect such changes is faced with a few challenges. (i) Very shallow gaps are needed in order to maximize the capacitance of the device; (ii) Parasitic capacitances between the readout electrodes need to be as small as possible to improve the signal to noise ratio; (iii) The surface should be flat and adhesive to facilitate the transfer of graphene; (iv) Additionally, to keep the pressure in the reference cavity constant, the cavity needs to be hermetically sealed by the graphene membrane. To address these challenges, we develop a device with electrical readout fabricated on top of a quartz substrate, which substantially reduces the parasitic capacitance of the electrical circuitry. To demonstrate the sensing concept, we transfer a few-layer graphene flake on top of the device and we use external gas

pressure load to deflect the drum, reading out the corresponding change in the capacitance.

A 3D schematic of the proposed device is shown in Fig. 1(a). The capacitor consists of a circular electrode on the bottom and a suspended few-layer (FL) graphene drum on top, forming a sealed cavity. The bottom electrode runs underneath a dielectric layer of spin-on-glass (SOG), which separates it from the top metal electrode. The drum is mechanically supported by the top electrode, which also serves as an electrical contact to the graphene. Figure 1(b) shows the sensing principle: when the pressure inside the cavity (P_{in}) is equal to the outside pressure (P_{out}), the capacitance of the device is given by the parallel plate capacitor formed by the graphene and the bottom electrode: C_0. When the outside pressure is higher than the pressure inside the cavity, this results in a positive pressure difference across the membrane, causing it to bulge downwards, which manifests itself as an increase of the measured capacitance. Conversely, if the pressure inside the cavity is higher than the outside pressure, the drum bulges upwards, resulting in a decrease of the measured capacitance.

Fabrication requires two e-beam lithography steps for the bottom and top electrodes. Both lithographic steps use two layers of PMMA resist (A6 495K [300 nm] and A3 950K [100 nm]) in order to create sloped resist walls which facilitate the lift-off. To minimize charging effects during the e-beam patterning, a 10 nm layer of Au is sputtered on top of the resist prior to the e-beam exposure. The Au layer is removed before developing the resist using KI/I_2 gold etchant. Figure 2(a) shows a sketch of the sample after developing the resist in MIBK:IPA (1:3) and evaporating 5 nm of titanium (5 nm) and 60 nm of gold-palladium ($Au_{0.6}Pd_{0.4}$) to form the bottom electrode. The titanium is used as an adhesion layer and is not shown in the figure.

After lift-off (Fig. 2(b)), a layer of FOX XR-1451 spin-on-glass (SOG) is spin-coated on the chip. In order to improve the conformity of the SOG layer to the underlying surface, the SOG layer is baked in two stages: 3 minutes at 150 °C and 3 minutes at 250 °C. Subsequently, the chip is placed in a N_2 furnace at 500 °C at 1 atm, which cures the SOG, making it

mechanically harder and also improving its surface smoothness and step coverage (Fig. 2(c)). The baking and curing processes are essential for obtaining a flat and smooth surface, which is important, as it largely influences the roughness of the electrode evaporated on top of it. Smooth surfaces enhance adhesion and thereby facilitate the transfer of graphene. The current process flow results in a cavity depth of 110 nm. The top electrodes are fabricated on top of the SOG layer, following the same steps of Fig. 2(a-b), with a different combination of metals: Ti/$Au_{0.6}Pd_{0.4}$/Cr (5 nm/90 nm/30). This is shown in Fig. 2(d). The AuPd yields lower surface roughness than pure gold and therefore provides for better adhesion of the graphene. The top layer of chromium is used as a hard mask for the following etching step, to avoid contamination of the underlying AuPd.

Fig. 2(e) shows the formation of the cavities by using reactive ion etching (RIE) of the SOG everywhere around the top electrodes. This is done at 7 μbar in CHF_3:Ar (50:2.5 sccm). The remaining Cr is then etched away using Cr etchant, which results in the final device (Fig. 2 (f)). The cavity depth can be easily tuned by changing the thickness of the top layer of AuPd. In Fig. 2(g) we show a false-colored SEM image of the device after the removal of the Cr. The bottom panel shows a zoom-in of the interface between the two electrodes (yellow) and the SOG layer in between (blue). After the device has been fabricated, graphene flakes (exfoliated from highly oriented pyrolytic graphite (HOPG) crystals) are transferred on top of the cavities using an all-dry transfer technique.[20] The resulting graphene drums are 5 μm in diameter.

The measurement setup is shown in Fig. 3. The device is mounted in a vacuum chamber connected to a membrane pump and a pressure controller. The pressure controller is connected to a N_2 gas bottle (purity 99.999 %) and the pressure of the gas inside the chamber can be controlled linearly by using a 0-10 V input voltage. The pressure controller has a voltage output, which enables a direct readout of the pressure inside the chamber. In this configuration, the pressure can be regulated between 1-1000 mbar (0-10 Volts on the input) with a resolution of $\approx$ 0.5 mbar. The capacitance of the graphene drum is measured using

an LCR meter in a two-port configuration. All capacitance measurements are performed at a frequency of 1 MHz with a voltage amplitude of $V_{\mathrm{p}} = 100$ mV. The integration time for the capacitance readout is 1500 ms. The inset of Fig. 3 shows an optical image of the measured device: a 6 nm - thick graphene drum.

RESULTS AND DISCUSSION

The measurement scheme is sketched in Fig. 4(a). Although graphene hermetically seals off the cavity, slow gas permeation usually takes place through its edges or through the underlying oxide.[21] We make use of this observation and keep the sample in vacuum for 48 h prior to each measurement to ensure that the gas from the cavity is completely evacuated ($P_{\mathrm{in}} \approx 0$). Then a square wave is applied to the control input of the pressure controller, such that the pressure in the chamber (P_{out}) is changed in a step-like fashion. It is worth noting that the rise time of the pressure in the chamber is typically faster than the sampling time (less than a second), whereas the time it takes to pump down the chamber to vacuum (1 mbar) is typically 2-4 seconds, depending on the height of the applied pressure step (P_{max}). Figure 4(b) shows the measured capacitance of the device as a function of time for two values of the pressure step height: $P_{\mathrm{max}} = 600$ mbar (blue) and 250 mbar (red). Both graphs show that the capacitance rises when the pressure inside the chamber P_{out} increases, and jumps back to the initial value upon pumping down. Despite the care taken to eliminate parasitic capacitances, by using a quartz substrate and local gate, the total capacitance of the device is ≈ 590 fF, mostly stemming from the parasitic capacitance of the wiring and the on-chip inter-electrode capacitance, since the contribution of the graphene drum is calculated to be only 1.58 fF.

Starting from $P_{\mathrm{in}} = P_{\mathrm{out}}$ and assuming an abrupt change in P_{out}, such that permeation effects can be neglected, the expected capacitance change can be calculated using an implicit

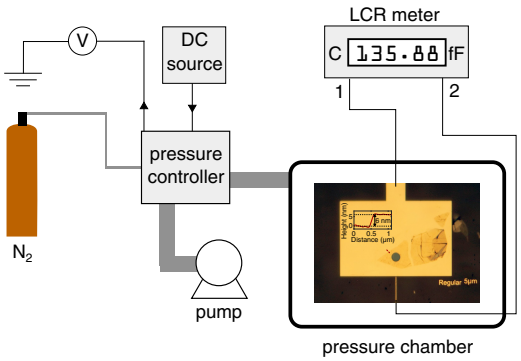

Figure 3: Schematic of the measurement setup: the device is mounted in a pressure chamber connected to a pressure controller with a DC voltage control input. The voltage output of the pressure controller is proportional to the actual pressure inside the chamber (P_{out}). The capacitance of the drum is read out using an LCR meter. The figure shows an optical image of the device: a FL graphene drum with a thickness of 6 nm. The thickness was determined using Atomic Force Microscopy (AFM) and the height profile along the red dashed line is shown in the inset of the figure.

relation between the pressure difference across the membrane (ΔP) and the deflection of the membrane's center (z):[22]

$$\Delta P = \frac{4n_0}{R^2}z + \frac{8Eh}{3R^4(1-\nu)}z^3, \tag{1}$$

where n_0 is the pre-tension of the membrane, R and h are its radius and thickness respectively and E and ν are the Young's modulus and the Poisson's ratio of the material. Knowing z and the spherical deformation shape of the membrane ($U(r) = z(1 - \frac{r^2}{R^2})$), the capacitance can be calculated using the parallel plate approximation as:

$$C = 2\pi\varepsilon_0 \int_0^R \frac{r}{g_0 - U(r)} dr, \tag{2}$$

where ε_0 is the vacuum permittivity and g_0 is the gap size. Using n_0 = 0.1 N/m and E = 1 TPa (values similar to the ones reported in literature[25]), the value of the extracted capacitance steps matches well with the numbers expected from theory. A measurement on a similar device (see Supporting Information Section I) shows comparable response to the ones shown in Fig. 4 (b), also in accordance with theory. On top of the measured signal, we also measure a slow drift of the capacitance over time (see Fig. 4). The cause of the

drift is not well understood and it might be due to a combination of slow gas leakage and condensation of humidity on the electrodes [23] or on the graphene membrane itself.[24]

Using pressure pulses of increasing height we can trace out a dependence of the capacitance change on the pressure difference across the membrane. To do so, we employ a measurement protocol sketched in the inset of Fig. 5(a). The sample is kept at vacuum (for 48 h prior to the measurement) and short pressure steps (10 s) are applied to the sample chamber, followed by 90 s of pumping, to ensure that the cavity underneath the graphene is pumped down to vacuum before applying the next pressure step. This way, it can be safely assumed that the height of the pressure step corresponds to the actual pressure difference felt by the graphene membrane. The opposite applies for the left side of the graph (blue curve): the sample is kept at 1 bar(for 48 h prior to the measurement) and pressure steps of the opposite sign are applied, followed by 90 s of ambient pressure. The measured capacitance change ΔC is plotted in the bottom panel of Fig. 5(a). The aforementioned drift was subtracted for this dataset after fitting it with a polynomial (see Supporting Information Section II).

The capacitance change is recorded as the height of the step in the measured capacitance immediately after applying the pressure pulse. Doing this for the entire span of ΔP (from -1 to +1 bar) we get a ΔC vs. ΔP curve, plotted in Fig. 5(b). The error bars at each point correspond to the RMS noise of the signal in the vicinity of the pressure step, as a measure of the uncertainty of the step determination. The black curve is the modeled response of the system for a 6 nm thick graphene membrane with a Young's modulus of 1 TPa. The model is in a good agreement with the measured response, providing further evidence that the signal is indeed coming from the displacement of the membrane. Thanks to the relatively low parasitic capacitances, despite the present drift, capacitance changes down to 50 aF could be distinguished.

The resolution of the measurement setup is limited by the resolution of the LCR meter, which is 10 aF. This corresponds to a pressure resolution of $\approx$ 360 Pa (or 0.36 mbar) for

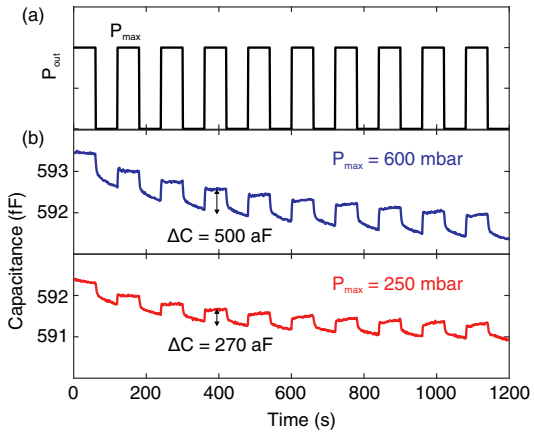

Figure 4: (a) Experimental procedure: the pressure is changed from vacuum to $P_{\max}$ with a period of 120 s. (b) Capacitance of the device as a function of time for two different runs using $P_{\max} = 600$ mbar (top) and $P_{\max} = 250$ mbar (bottom). Both panels show the extracted capacitance step height (ΔC) at the moment of changing the pressure.

$\Delta P \approx 0$ and 10.6 kPa (or 106 mbar) for $\Delta P = 1$ bar. For potential application of such device as a pressure sensor, it is interesting to look at the responsivity of the device around $\Delta P = 0$. By design, the responsivity of the presented device peaks at around 0.1 aF/Pa at 0 mbar pressure difference (see Supporting Information Section III). The root-mean-square (RMS) noise of the measurement setup is 25 aF/$\sqrt{\text{Hz}}$. However, due to the drift present in the measurements, the minimal step height that could be resolved was 50 aF. The relative error of the pressure measurement ranges from 0.6 % (for $\Delta P \approx 1$ bar) all the way up to 300 % for $-100\,\text{mbar} < \Delta P < 100\,\text{mbar}$. The accuracy of the sensor can also be influenced by morphological imperfections of the membrane itself. There are multiple ways to increase the responsivity of the device: decreasing the thickness of the graphene (h), decreasing the pre-tension of the membrane (n_0), increasing its radius (R), or connecting N such devices in parallel. A detailed analysis of the influence of each parameter on the responsivity of the device are shown in the Supporting Information Section III. According to the calculations, changing the thickness h does not drastically influence the responsivity. Increasing R or reducing the pre-tension n_0 improve the responsivity by one or two orders of magnitude. We note that controlling n_0 is challenging, since it is largely determined by the transfer process and usually exhibits large spreads.[25] Moreover, making devices with larger radii and lower

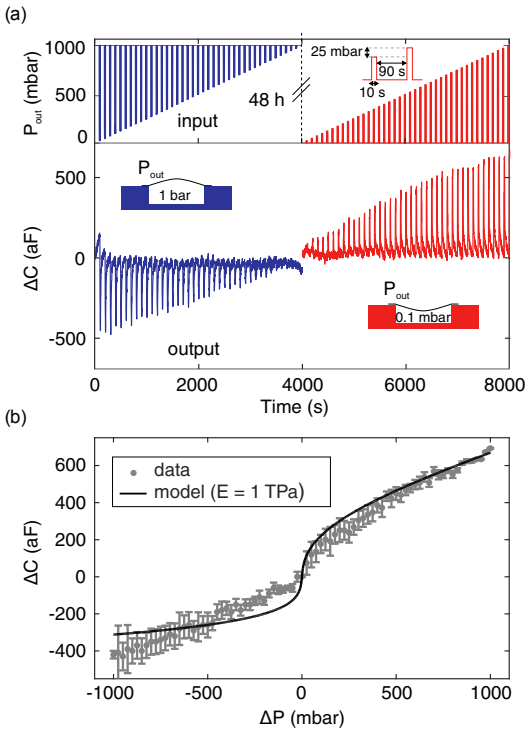

Figure 5: (a) Capacitance change as a function of time (top). Bottom: Starting from 1 bar, pressure is changed in a stepwise fashion with increasing steps of 25 mbar (10 % pulse duration with a 100 s period). The chamber is then pumped down to 1 mbar and a similar procedure is repeated with the chamber being pumped to vacuum after each step. (b) The extracted values for ΔC as a function of the applied pressure difference across the membrane (gray dots). A theoretical fit to the data using the device dimensions, with pre-tension $n_0 =$ 0.1 N/m and Young's modulus E = 1 TPa.

pre-tension would impair the yield of the devices[26] and reduce their dynamic range (due to collapse of the membrane at high ΔP). A viable optimization route would be increasing the number of drums connected in parallel (N) which would improve the responsivity of the device, since the total capacitance of the device would increase by a factor of N. With more than 1000 drums in parallel (resulting roughly in a chip size of 100 x 100 μm) one could push the responsivity to values higher than 100 aF/Pa, resulting in a 0.1 Pa resolution using the same measurement setup.

To demonstrate the feasibility of capacitive readout of the graphene sensor with an integrated circuit, we replaced the LCR meter with an Analog Devices (AD7746) capacitance-to-digital converter chip (with dimensions 5x5 mm^2) which we interfaced through using the built-in I2C protocol library of an Arduino. We show an example of such measurement in

the Supporting Information Section IV. Even though the signal-to-noise of this measurement is an order of magnitude worse than the one using the LCR meter, it still serves as a proof-of-principle that on-chip detection of small capacitance changes can be realized using commercial electronic devices.

The drift in the measurement together with the poor hermeticity of the membrane hamper the long-term stability of the device. For its commercial application as a pressure sensor, the hermeticity of the device needs to be improved (e.g. by properly sealing the membrane edges) and the cross-sensitivity to the environment (humidity/gas composition) needs to be investigated more thoroughly.

CONCLUSION

In conclusion, we demonstrate on-chip capacitive readout of a single suspended graphene drum. To obtain the responsivity required for sensing such small capacitance changes, the entire fabrication is done on an insulating quartz substrate, minimizing the parasitic capacitance of the readout electrodes. We use uniform pressure load to statically deform the membrane, which results in a capacitance change of the device. Using this method, we are able to read out capacitance changes down to 50 aF and detect pressure steps down to 25 mbar. The height of the steps is consistent with predictions from the theoretical model. We also traced out a force-deflection curve by pulsing the pressure in the chamber with pulses of increasing height. The measured ΔC vs. ΔP curve matched well with theory, based on a graphene membrane with a Young's modulus of 1 TPa. We also measured a temporal drift in the capacitance, possibly originating from residual humidity in the chamber. This work is aimed at probing the limit of static capacitive detection of graphene nanodrums. We optimized the device to enable detection of very small capacitance changes of down to 50 aF.

By combining this device design with an on-chip capacitance-to-digital converter we show a proof-of-concept demonstration of the feasibility of integrating suspended 2D membranes into nanomechanical pressure sensors.

ASSOCIATED CONTENT

Supporting Information

Measurements on a second device, method of drift subtraction, calculations of the expected responsivity of the device as a function of varying parameters, and capacitive readout using an AD7746 capacitance-to-digital converter.

ACKNOWLEDGMENTS

This work was supported by the Netherlands Organisation for Scientific Research (NWO/OCW), as part of the Frontiers of Nanoscience (NanoFront) program and the European Union Seventh Framework Programme under grant agreement n° 604391 Graphene Flagship.

References

(1) Smith, A. D.; Niklaus, F.; Paussa, A.; Vaziri, S.; Fischer, A. C.; Sterner, M.; Forsberg, F.; Delin, A.; Esseni, D.; Palestri, P.; stling, M.; Lemme, M. C. Electromechanical Piezoresistive Sensing in Suspended Graphene Membranes. *Nano Letters* **2013**, *13*, 3237–3242, PMID: 23786215.

(2) Smith, A. D.; Vaziri, S.; Niklaus, F.; Fischer, A.; Sterner, M.; Delin, A.; Östling, M.;

Lemme, M. Pressure Sensors Based on Suspended Graphene Membranes. *Solid-State Electronics* **2013**, *88*, 89 – 94.

(3) Dolleman, R. J.; Davidovikj, D.; Cartamil-Bueno, S. J.; van der Zant, H. S. J.; Steeneken, P. G. Graphene Squeeze-Film Pressure Sensors. *Nano Letters* **2016**, *16*, 568–571.

(4) Smith, A. D.; Niklaus, F.; Paussa, A.; Schrder, S.; Fischer, A. C.; Sterner, M.; Wagner, S.; Vaziri, S.; Forsberg, F.; Esseni, D.; stling, M.; Lemme, M. C. Piezoresistive Properties of Suspended Graphene Membranes under Uniaxial and Biaxial Strain in Nanoelectromechanical Pressure Sensors. *ACS Nano* **2016**, *10*, 9879–9886, PMID: 27797484.

(5) Chen, Y.-M.; He, S.-M.; Huang, C.-H.; Huang, C.-C.; Shih, W.-P.; Chu, C.-L.; Kong, J.; Li, J.; Su, C.-Y. Ultra-large Suspended Graphene as a Highly Elastic Membrane for Capacitive Pressure Sensors. *Nanoscale* **2016**, *8*, 3555–3564.

(6) Patel, R. N.; Mathew, J. P.; Borah, A.; Deshmukh, M. M. Low Tension Graphene Drums for Electromechanical Pressure Sensing. *2D Materials* **2016**, *3*, 011003.

(7) Koenig, S. P.; Wang, L.; Pellegrino, J.; Bunch, J. S. Selective Molecular Sieving Through Porous Graphene. *Nature Nanotechnology* **2012**, *7*, 728–732.

(8) Wang, L.; Drahushuk, L. W.; Cantley, L.; Koenig, S. P.; Liu, X.; Pellegrino, J.; Strano, M. S.; Bunch, J. S. Molecular Valves for Controlling Gas Phase Transport Made from Discrete Ångström-sized Pores in Graphene. *Nature nanotechnology* **2015**, *10*, 785–790.

(9) Dolleman, R. J.; Cartamil-Bueno, S. J.; van der Zant, H. S. J.; Steeneken, P. G. Graphene Gas Osmometers. *2D Materials* **2016**, *4*, 011002.

(10) Chen, C.; Rosenblatt, S.; Bolotin, K. I.; Kalb, W.; Kim, P.; Kymissis, I.; Stormer, H. L.; Heinz, T. F.; Hone, J. Performance of Monolayer Graphene Nanomechanical Resonators with Electrical Readout. *Nature Nanotechnology* **2009**, *4*, 861–867.

(11) Xu, Y.; Chen, C.; Deshpande, V. V.; DiRenno, F. A.; Gondarenko, A.; Heinz, D. B.; Liu, S.; Kim, P.; Hone, J. Radio Frequency Electrical Transduction of Graphene Mechanical Resonators. *Applied Physics Letters* **2010**, *97*, 243111.

(12) Chen, C. *Graphene NanoElectroMechanical Resonators and Oscillators*; Columbia University, 2013.

(13) Weber, P.; Gttinger, J.; Tsioutsios, I.; Chang, D. E.; Bachtold, A. Coupling Graphene Mechanical Resonators to Superconducting Microwave Cavities. *Nano Letters* **2014**, *14*, 2854–2860, PMID: 24745803.

(14) Singh, V.; Bosman, S.; Schneider, B.; Blanter, Y. M.; Castellanos-Gomez, A.; Steele, G. Optomechanical Coupling Between a Multilayer Graphene Mechanical Resonator and a Superconducting Microwave Cavity. *Nature nanotechnology* **2014**, *9*, 820–824.

(15) Song, X.; Oksanen, M.; Li, J.; Hakonen, P.; Sillanpää, M. A. Graphene Optomechanics Realized at Microwave Frequencies. *Physical review letters* **2014**, *113*, 027404.

(16) Bunch, J. S.; Van Der Zande, A. M.; Verbridge, S. S.; Frank, I. W.; Tanenbaum, D. M.; Parpia, J. M.; Craighead, H. G.; McEuen, P. L. Electromechanical Resonators from Graphene Sheets. *Science* **2007**, *315*, 490–493.

(17) Castellanos-Gomez, A.; van Leeuwen, R.; Buscema, M.; van der Zant, H. S. J.; Steele, G. A.; Venstra, W. J. Single-Layer MoS_2 Mechanical Resonators. *Advanced Materials* **2013**, *25*, 6719–6723.

(18) AbdelGhany, M.; Ledwosinska, E.; Szkopek, T. Theory of the suspended graphene varactor. *Applied Physics Letters* **2012**, *101*, 153102.

(19) AbdelGhany, M.; Mahvash, F.; Mukhopadhyay, M.; Favron, A.; Martel, R.; Siaj, M.; Szkopek, T. Suspended Graphene Variable Capacitor. *2D Materials* **2016**, *3*, 041005.

(20) Castellanos-Gomez, A.; Buscema, M.; Molenaar, R.; Singh, V.; Janssen, L.; van der Zant, H. S. J.; Steele, G. A. Deterministic Transfer of Two-Dimensional Materials by All-Dry Viscoelastic Stamping. *2D Materials* **2014**, *1*, 011002.

(21) Bunch, J. S.; Verbridge, S. S.; Alden, J. S.; van der Zande, A. M.; Parpia, J. M.; Craighead, H. G.; McEuen, P. L. Impermeable Atomic Membranes from Graphene Sheets. *Nano Letters* **2008**, *8*, 2458–2462.

(22) Bunch, J. S. *Mechanical and Electrical Properties of Graphene Sheets*; Cornell University Ithaca, NY, 2008.

(23) Ford, L. The Effect of Humidity on the Calibration of Precision Air Capacitors. *Journal of the Institution of Electrical Engineers-Part II: Power Engineering* **1948**, *95*, 709–712.

(24) Olson, E. J.; Ma, R.; Sun, T.; Ebrish, M. A.; Haratipour, N.; Min, K.; Aluru, N. R.; Koester, S. J. Capacitive Sensing of Intercalated H_2O Molecules Using Graphene. *ACS Applied Materials & Interfaces* **2015**, *7*, 25804–25812, PMID: 26502269.

(25) Lee, C.; Wei, X.; Kysar, J. W.; Hone, J. Measurement of the Elastic Properties and Intrinsic Strength of Monolayer Graphene. *Science* **2008**, *321*, 385–388.

(26) Cartamil-Bueno, S. J.; Centeno, A.; Zurutuza, A.; Steeneken, P. G.; van der Zant, H. S. J.; Houri, S. Very Large Scale Characterization of Graphene Mechanical Devices Using a Colorimetry Technique. *Nanoscale* **2017**, *9*, 7559–7564.

Graphical TOC Entry